PROJECTING LULC CHANGE (2025–2039) AND MODELING LANDSLIDE SUSCEPTIBILITY USING CELLULAR AUTOMATA–MARKOV CHAIN (CA–MC) IN THE KAMBANG WATERSHED, WEST SUMATRA, INDONESIA

Triyatno TRIYATNO [1*], Lailatur RAHMI [1], Syafri ANWAR [1], Beni AULIA [1] and Sumayyah Aimi Mohd NAJIB [2]

DOI: 10.21163/ GT_2026.212.01

ABSTRACT

This study aims to map and quantify Land Use/Land Cover (LULC) change across 2025, 2029, and 2039 to develop a Frequency Ratio (FR) based landslide hazard model, to integrate LULC projections with key environmental parameters, and to delineate priority hotspot areas for mitigation based on scenario-specific susceptibility patterns. This study applies a quantitative, spatial approach to examine how LULC change reshapes landslide risk. Supervised classification was performed to produce the 2025 LULC map, which serves as the base year for projection. Future LULC (2029, 2039) was simulated using Cellular Automata–Markov Chain (CA–MC) formulations. A Random Forest (RF) model was used to predict Landslide Potential (LP) based on environmental variables and distance to mapped landslides. The results show primary forest is projected to decline steadily across the 2025, 2029, and 2039 years. The LULC maps achieve overall accuracies of 0.92 (2025), 0.88 (2029), and 0.86 (2039). The high-hazard class increases from 4,273.29 ha (8.90%) in 2025 to 4,782.06 ha (9.96%) in 2029 (+508.77 ha; +1.06 percentage points), and to 5,041.89 ha (10.50%) in 2039 (+259.83 ha; +0.54 percentage points). Combined, the moderate + high categories grow from 10,271.25 ha (21.39%) in 2025 to 15,590.11 ha (32.47%) in 2029 (+5,318.86 ha; +11.08 percentage points), and to 16,155.00 ha (33.65%) in 2039 (+564.89 ha; +1.18 percentage points). Landslide-potential models yield Area Under the Curve (AUC) of 0.95 (2025), 0.87 (2029), and 0.84 (2039). The results indicate a clear and coherent trajectory linking LULC change to evolving landslide susceptibility in the Kambang watershed. To mitigate future risks, priority actions should include protecting steep-slope forests, deploying deep-rooted revegetation and targeted slope stabilization, upgrading surface–subsurface drainage on hillslopes and along access roads, and incorporating the 2025/2029/2039 susceptibility maps into risk-sensitive spatial planning.

Keywords: *LULC; Landslide; Susceptibility; Cellular Automata–Markov Chain (CA–MC); Random Forest; Watershed.*

1. INTRODUCTION

Recent global environmental change is accelerating transformations that reverberate through human systems and ecosystems, and Land Use/Land Cover (LULC) dynamics are central to these shifts (Naeem et al., 2025; Van Toor et al., 2024; Beroho et al., 2025; Ikhwan et al., 2025). Human-driven LULC alters surface energy and moisture exchanges, redirects hydrological responses, and can undermine ecological stability, which is increasingly documented through advances in classification, fraction estimation, and spatiotemporal mapping (Patel et al., 2024; Febriandi et al., 2025).

---

[1]*Department of Geography, Universitas Negeri Padang, Padang, Indonesia. *Corresponding author: triyatno@fis.unp.ac.id (TT); lailaturrahmi@student.unp.ac.id (LR); syafri.anwar.fis@gmail.com (SA); beniaulia@fis.unp.ac.id (BA)*

[2]*Department of Geography and Environment, Faculty of Human Sciences, Sultan Idris Education University, Malaysia. sumayyah@fsk.upsi.edu.my (SAMN)*

The resulting disasters impose substantial costs, including damage to assets, interruptions to livelihoods, and, at worst, loss of life, which underscores the need to anticipate how today's LULC trajectories may shape tomorrow's hazard landscape (Chowdhury et al., 2024; Es-smairi et al., 2023).

Among the hazard types that are most sensitive to LULC and extreme rainfall, landslides are particularly prominent. Vegetation removal, slope modification, and altered drainage pathways can destabilize hillslopes, and the impacts often peak during wet seasons and in forested terrains where management choices strongly influence outcomes (Asada et al., 2024; Asmare, 2023). In many tropical settings, intense precipitation coincides with steep relief and rapid land transformation, which creates recurrent susceptibility hotspots that threaten communities and critical lifelines (Chowdhury et al., 2024; Es-smairi et al., 2023). These conditions motivate integrated assessments that connect evolving land mosaics to spatiotemporal changes in slope stability.

Situated immediately south of Padang City in Pesisir Selatan Regency, the Kambang River Basin exemplifies these challenges. Recurrent landslides disrupt mobility along the western corridor that links West Sumatra and Bengkulu, and they also result in fatalities and property losses in exposed settlements. The areas of Kambang Utara and Kambang Timur are frequently affected, which highlights the need for site-specific analysis and forward-looking planning that can guide both local preparedness and regional connectivity strategies. Because consequences in Kambang span household damages and interprovincial flows, the basin constitutes a priority landscape for integrated hazard assessment and targeted mitigation. A substantial body of literature addresses each component of this problem. On the LULC side, recent work advances prediction and monitoring through Cellular Automata–Markov Chain (CA–MC) and machine-learning pipelines, remote-sensing fraction estimation, and multi-scenario coupling with climate and hydrology models (Girma et al., 2022; Naeem et al., 2025; Beroho et al., 2025; Febriandi et al., 2025; Ikhwan et al., 2025). On the landslide side, studies compare and combine statistical and machine-learning approaches, including Frequency Ratio (FR). Shannon entropy, logistic regression, Random Forest (RF), and ensemble evidence frameworks to map susceptibility and evaluate model skill (Es-smairi et al., 2023; Chowdhury et al., 2024; Roy et al., 2023). Despite these advances, a notable gap persists because LUCC modeling and landslide mapping are often performed in parallel rather than explicitly linked so that projected LULC under future time years can drive dynamic susceptibility updates and reveal risk frontiers under plausible landscape trajectories (Triyatno et al., 2023).

This study responds to that gap by integrating forward LULC projections with landslide hazard modeling for the Kambang watershed. Multiple years, namely 2025, 2029, and 2039, capture near-term, medium-term, and longer-term trajectories that are consistent with planning cycles, while environmental variables represent controlling factors for slope stability and runoff. By coupling projected land transformations with hazard estimates, the analysis identifies where susceptibility may intensify, remain stable, or diminish, and this information supports the timing and prioritization of interventions such as vegetation management, slope stabilization, drainage improvements, and land-use regulation (Roy et al., 2023; Asada et al., 2024). The practical value is twofold, because communities in Kambang Utara and Kambang Timur can use forward-looking maps to prepare ahead of peak rainy seasons. Local as well as provincial authorities can target spatial planning, infrastructure maintenance, and investment in ways that steadily reduce exposure and vulnerability (Chowdhury et al., 2024; Es-smairi et al., 2023). Accordingly, this study aims to map and quantify LULC change across 2025–2029–2039, to develop an FR-based landslide hazard model, to integrate LULC projections with key environmental parameters, and to delineate priority hotspot areas for mitigation based on scenario-specific susceptibility patterns. The novelty of this study lies in the dynamic coupling of forward LULC projections generated by a CA–MC framework with landslide-susceptibility modeling (FR/RF) at matched planning years (2025, 2029, 2039). In contrast to studies that treat LUCC and landslide mapping separately or at a single year without feeding projected mosaics into hazard models, this approach explicitly links projected land-change trajectories to evolving hazard and validates the chain year by year.

2. STUDY AREA

The study was conducted in the Kambang watershed of Pesisir Selatan Regency, immediately south of Padang City (West Sumatra, Indonesia). The basin extends between approximately 100°41'00"–100°57'30" E and 1°47'00"–1°37'00" S, covering 48,014.55 ha. The watershed contains steep headwater hillslopes and lower-relief footslopes and valley floors where settlements are. Topographically, the basin is characterized by dissected terrain with steep to very steep slopes in the uplands and gentler surfaces in the downstream piedmont/valley areas. Elevation varies markedly from near sea level to ~2,020 MASL, reflecting strong relief that channels runoff and focuses mass-movement processes on hillslopes. The watershed includes settlements such as Kambang Utara and Kambang Timur and forms part of the western transport corridor connecting West Sumatra and Bengkulu. Recurrent landslides along steep, dissected hillslopes disrupt mobility and threaten lives and assets, making the Kambang basin a priority landscape for scenario-based hazard assessment and forward-looking mitigation. More details can be seen in **figure 1** below.

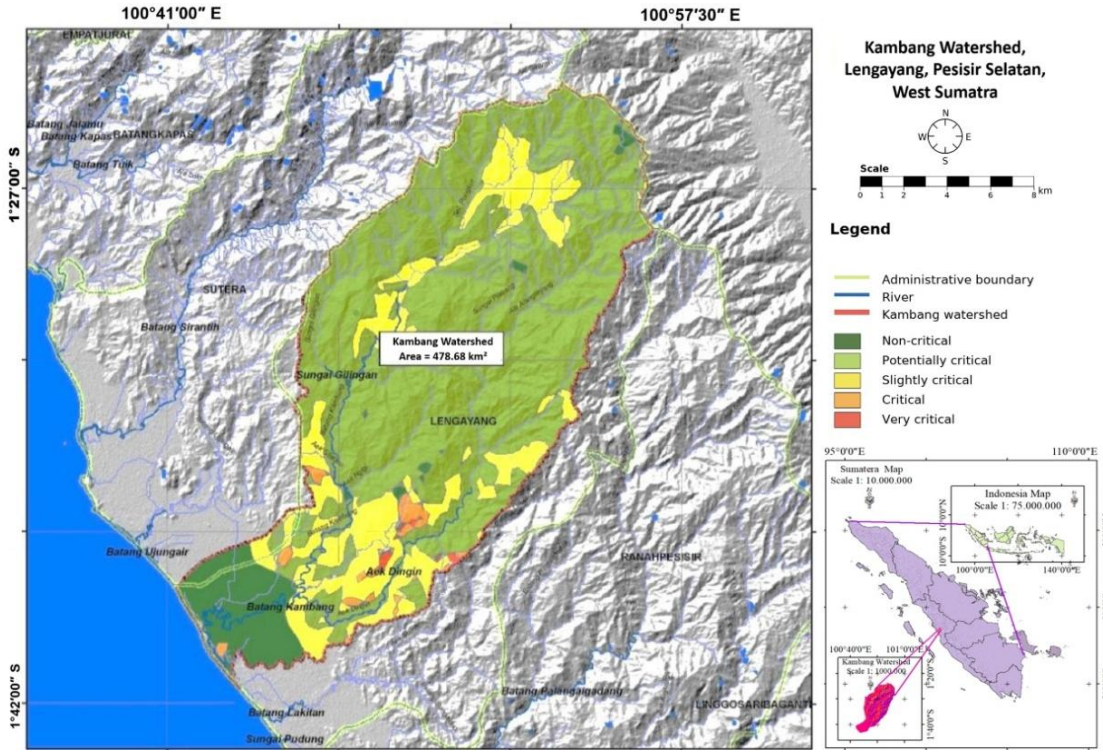

Fig. 1. Study area map of the Kambang Watershed showing administrative boundaries and rivers.

3. METHODS

This study applies a quantitative, spatial approach to examine how LULC change reshapes landslide risk (Febriandi et al., 2025). The work was carried out in the Kambang watershed, ~120 km from Padang City, West Sumatra. Quantitatively, class-level influences are estimated with FR using the landslide inventory and conditioning factors (slope, rainfall, geology, geomorphology, soil), susceptibility is evaluated with AUC, and LULC projections for 2025/2029/2039 are produced via CA–MC. Spatially, these statistical relationships are applied cell-by-cell to create a baseline surface, then re-run with each projected LULC to generate year-specific susceptibility maps and quantify the reallocation among low–medium–high classes. Risk reshaping is summarized by area changes (Δ)

and hotspots where susceptibility increases especially where forest converts to oil palm/mixed orchard/dryland agriculture on steeper terrain. To maintain scope clarity, the FR-based Landslide Hazard Surface (LHS) (knowledge-driven) and the RF-based Landslide Potential (LP) model (data-driven) are treated as distinct products, and their agreement is explicitly compared.

3.1. Study setting and workflow

The study followed three stages. More details are explained as follows.

Pre-field. Compiled multi-temporal satellite imagery and ancillary data to build the LULC baseline and the environmental layers used in modeling. The image archive consisted of Landsat 5 (2000), Landsat 7 (2009), Landsat 8 (2019), and Landsat 9 (2025) scenes. Supervised classification was performed to produce the 2025 LULC map, which serves as the base year for projection. Supporting datasets included geology, geomorphology, soil, a Digital Elevation Model (DEM) (for slope, elevation, and contours), and rainfall. These layers were also prepared for FR analysis and the landslide hazard map. All rasters were co-registered and resampled to a common grid/resolution to avoid spatial misalignment in subsequent modeling.

Field. Documented landslide occurrences and collected inventory points and ground samples in areas affected by natural landslides. These data were used both to validate the FR-based landslide hazard and to train/validate the prediction model of LP by comparing the mapped hazard/potential with observed landslide points. To reduce positional bias, each inventory point was buffered by the median mapping uncertainty before sampling environmental covariates.

Post-field. With 1) projected near-term and longer-term LULC trajectories to 2029 and 2039 with a CA–MC model; 2) computed FR values for each conditioning factor and produced a LHS; 3) developed a RF prediction of LP using environmental variables and the landslide inventory; and 4) assessed accuracy of both LULC and landslide-potential outputs. Training/validation used spatial block cross-validation, and classification thresholds were selected on the precision–recall curve to handle class imbalance.

3.2. Data analysis

LULC change modeling (CA–MC)

Future LULC (2029, 2039) was simulated using CA–MC formulations (Badrakh et al., 2025; Beroho et al., 2025; Kubacka et al., 2025). A transition probability matrix P was estimated from historical LULC (Mondal et al., 2016; Murmu et al., 2025), and neighborhood effects were introduced via the cellular automata with formula.

$$\mathbf{S_{t+1} = f(S_t, N)S_{t+1} = P \,.\, S_tP = [p_{ij}]} \tag{1}$$

where $\mathbf{S}$ is set of LULC states, $\mathbf{N}$ neighborhood, and $\mathbf{p_{ij}}$ transition probability from class $\mathbf{i}$ **to** $\mathbf{j}$. Calibration used 2000→2009 and 2009→2019; validation used 2019→2025; Neighborhood and suitability constraints (slope, distance-to-roads/settlements) limited implausible transitions.

LULC accuracy assessment

Next for computed Overall Accuracy (OA), User's Accuracy (UA), Producer's Accuracy (PA), and Kappa with formula.

$$\mathbf{OA} = \frac{\sum_{i}^{r=1} D_{ii}}{N}, \mathbf{UA_i} = \frac{D_{ii}}{x_{+i}}, \mathbf{PA_i} = \frac{D_{ii}}{x_{+i}}, \ \mathbf{OA} = \frac{N\sum_{i}^{r=1} D_{ii} - \sum_{i}^{r=1}(x_i + x_{+i})}{N^2 - \sum_{i}^{r=1}(x_i + x_{+i})} \tag{2}$$

Validation samples were stratified per class (≥50 points/class) to avoid rare-class under-representation.

Landslide hazard (FR)

At stage quantified the contribution of slope, rainfall, geology, geomorphology, and soil using the FR method (Asmare, 2023; Huang et al., 2024; Zhou et al., 2021) with formula.

$$\mathbf{FR} = \frac{(\textbf{landslide pixels in class})/(\textbf{pixels of class})}{\textbf{all landslide pixels / all pixels}} \quad (3)$$

FR values >1 indicate positive association with landslides; FR <1 indicates negative association. The Landslide-Susceptibility Map (LSM) was computed using the classic bivariate formulation: for each cell, the landslide score equals the sum of the log-FR across criteria (Σ ln FR). No subjective weighting was applied. To avoid double-counting and leakage when projecting with CA–MC, LULC is not included inside the FR combination. LULC effects are applied by re-evaluating susceptibility under projected classes with the following formula.

$$\mathbf{LSM} = \mathbf{0.30\ FR_{geology}} + \mathbf{0.30\ FR_{geomorphology}0.20\ FR_{soil}} + \mathbf{0.30\ FR_{geology}} + \mathbf{0.10\ FR_{rainfall}} + \mathbf{0.10\ LULC_n} \quad (4)$$

where $\mathbf{LULC_n}$ encodes projected LULC (2029 or 2039). See also Es-smairi et al., 2023; Ahmad et al., 2023 for related FR-based LSM applications.

Prediction model

RF was built on the landslide inventory and environmental predictors (Euclidean distance to landslide points, slope FR, soil FR, geology FR, geomorphology FR, elevation, contours, rainfall FR) following established practice (Talukdar et al., 2021; Shanley et al., 2021; Williams et al., 2025). To preserve methodological separation and prevent target leakage, RF inputs comprised slope, curvature, elevation, lithology/geomorphology/soil (one-hot), rainfall climatology, and distances to rivers/roads/faults, plus LULC class FR-derived layers were deliberately excluded. For interpretability, permutation and Gini importances were computed, and SHAP values were derived for the final RF, together with Partial Dependence (PD) and Accumulated Local Effects (ALE) plots for key drivers (slope, soil, geomorphology, distance-to-rivers/roads). RF offers strong performance with limited tuning, robustness to mixed/noisy predictors, and out-of-bag error for fast calibration, and RF is retained unless AUC-PR improves by ≥0.02 with boosting. Training/validation used spatial block cross-validation with class-weight balancing; decision thresholds were chosen at the F1/IoU-optimal point on the precision–recall curve.

4. RESULTS

4.1. LULC changes model

The LULC changes model shows projected in the Kambang watershed by integrating the current LULC distribution with observed transition trends. Class-level counts, areas, and percentages for each year (2025, 2029, 2039). More details can be seen in **table 1** below.

Primary forest is projected to decline steadily across the years 2025, 2029, and 2039. The area decreases from 36,742.23 ha (76.52%) in 2025 to 35,060.67 ha (73.02%) in 2029, resulting in a loss of 1,681.56 ha and a 3.50 percentage point decrease. By 2039, the primary forest is projected to be 33,310.80 ha (69.38%), indicating a further loss of 1,749.87 ha and a 3.64 percentage point decline relative to 2029. Secondary forest follows the same trend, declining from 4,070.07 ha (8.48%) in 2025 to 3,821.40 ha (7.96%) in 2029 and then to 2,858.04 ha (5.95%) in 2039, which corresponds to successive decreases of 248.67 ha (0.52 percentage points) and 963.36 ha (2.01 percentage points).

Oil palm shows the most pronounced gains. The area increases from 311.31 ha (0.65%) in 2025 to 1,347.03 ha (2.81%) in 2029, an increment of 1,035.72 ha and 2.16 percentage points, and then rises to 3,920.49 ha (8.17%) in 2039, adding 2,573.46 ha and 5.36 percentage points.

Table 1

LULC changes from 2025 to 2039.

LULC	LULC 2025			LULC 2029			LULC 2039		
	Count	Area (ha)	%	Count	Area (ha)	%	Count	Area (ha)	%
Primary forest	408,247	36,742.23	76.52	389,563	35,060.67	73.02	370,120	33,310.80	69.38
Secondary forest	45,223	4,070.07	8.48	42,460	3,821.40	7.96	31,756	2,858.04	5.95
Oil palm	3,459	311.31	0.65	14,967	1,347.03	2.81	43,561	3,920.49	8.17
Mangrove	48	4.32	0.01	48	4.32	0.01	48	4.32	0.01
Water bodies	2,750	247.50	0.52	2,750	247.50	0.52	2,750	247.50	0.52
Built-up land	8,885	799.65	1.67	8,888	799.92	1.67	8,905	801.45	1.67
Rice fields	24,710	2,223.90	4.63	24,710	2,223.90	4.63	24,710	2,223.90	4.63
Dryland agriculture	1,160	104.40	0.22	1,371	123.39	0.26	2,362	212.58	0.44
Bare land	4,464	401.76	0.84	4,436	399.24	0.83	3,741	336.69	0.70
Mixed orchard	34,549	3,109.41	6.48	44,302	3,987.18	8.30	45,542	4,098.78	8.54
TOTAL	533,495	48,014.55	100	533,495	48,014.55	100	533,495	48,014.55	100

Source: Data analysis, 2025.

Mixed orchard also grows, from 3,109.41 ha (6.48%) in 2025 to 3,987.18 ha (8.30%) in 2029 and 4,098.78 ha (8.54%) in 2039. These increases amount to 877.77 ha (1.82 percentage points) between 2025 and 2029 and 111.60 ha (0.24 percentage points) between 2029 and 2039. Dryland agriculture expands more modestly, from 104.40 ha (0.22%) in 2025 to 123.39 ha (0.26%) in 2029 and 212.58 ha (0.44%) in 2039, which equals gains of 18.99 ha (0.04 percentage points) and 89.19 ha (0.18 percentage points) across the two intervals. Built-up land shows negligible change (799.65 ha in 2025; 799.92 ha in 2029; 801.45 ha in 2039), with its share remaining about 1.67%. Rice fields are constant at 2,223.90 ha (4.63%) at all time points. Water bodies and mangrove areas are likewise stable at 247.50 ha (0.52%) and 4.32 ha (0.01%), respectively. Bare land declines gradually from 401.76 ha (0.84%) in 2025 to 399.24 ha (0.83%) in 2029 and 336.69 ha (0.70%) in 2039, which corresponds to decreases of 2.52 ha (0.01 percentage points) and 62.55 ha (0.13 percentage points).

Oil palm expansion concentrates on gentler terrain and valley floors where accessibility is higher. In contrast, conversions affecting forest classes are more common on dissected hillslopes, where mixed orchard and dryland agriculture extends into steeper gradients at elevations generally below 500 MASL. These spatial patterns indicate that continued forest loss on slopes is likely to reduce surface stability during peak rainy seasons. More details can be seen in **figure 2**.

The LULC maps achieve overall accuracies of 0.92 (2025), 0.88 (2029), and 0.86 (2039). Because all values exceed 0.85, the classifications meet a high-performance threshold and are suitable for use as inputs to the subsequent landslide-susceptibility modeling. **Figure 3** shows a persistent contraction of primary and secondary forests from 2025 to 2039, accompanied by rapid expansion of oil palm and a more gradual increase in mixed orchard and dryland agriculture, whereas rice fields, water bodies, and mangrove remain essentially unchanged. The spatial arrangement of these transitions, forest loss on slopes, and agricultural expansion on gentler terrain implies increasing exposure of unstable areas during peak rainy seasons. This interpretation is consistent with regional multi-criteria hazard zoning in the Tarusan watershed, where GIS mapping highlighted higher susceptibility along valley floors/low-lying zones under expanding agriculture and settlement, reinforcing the relevance of our valley-focused oil palm gains for future exposure (Barlian et al., 2025). Moreover, accurate terrain and exposure layers within a spatial framework materially improve spatial risk delineation for different hazard types with a couple of LULC projections with susceptibility modeling (Triyatno et al., 2024). In the study use the LULC projections are used as inputs to the hazard model to quantify where susceptibility is likely to intensify under the projected trajectories.

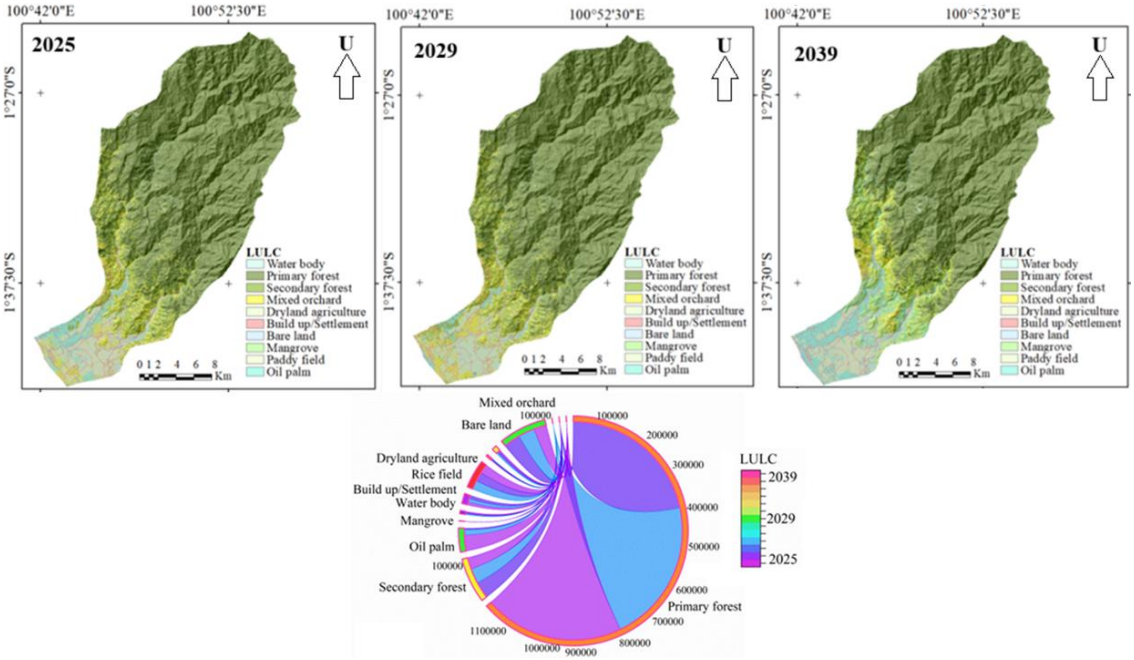

Fig. 2. Map of the spatial distribution of improved drinking water access before the disaster, showing the pipeline network (intake points, reservoirs, and transmission pipelines).

4.2. Landslide hazard

Landslide hazard indicates the potential of an area to experience landslides. In the Kambang watershed, it is governed by five conditioning factors, namely slope, rainfall, geology, geomorphology, and soil, whose class-level effects are summarized using the FR. By definition, FR > 1 shows a class that is more common within landslide locations than in the landscape overall (positive influence), whereas FR < 1 shows a class that is less associated with landslides (negative influence). More details can be seen in **figure 3** below.

As depicted in **figure 3**, FR ranges differ among factors: geology ≈ 0–1.50, geomorphology ≈ 0–1.59, slope ≈ 0–1.81, soil ≈ 0–1.81, and rainfall classes cluster around ≈ 0.61. These distributions indicate that slope and soil contain the strongest positively associated classes (up to ~1.81), followed by geomorphology (up to ~1.59) and geology (up to ~1.50). In contrast, the rainfall classes used here contribute a weaker standalone signal (≈0.61), suggesting that rainfall primarily operates as a trigger that amplifies instability where conditioning factors are already unfavorable. A high FR value in one class does not automatically translate into a proportionally high map-level hazard, because the effect also depends on that class's spatial prevalence (number of pixels) and its co-occurrence with other adverse classes. These patterns are consistent with prior evidence from Koto XI Tarusan, where slope-controlled morphometry dominated landslide impacts and lithology/landform acted as secondary controls (Triyatno et al., 2020).

In line with process-based findings in the Air Dingin Watershed in Padang where terrain steepness and potential failure conditions of soil erodibility, while rainfall primarily serves as energy input/trigger (Putra et al., 2025). Geological, geomorphological, and soil conditions also influence landslide occurrence in the study area. Weathered rock facilitates water infiltration, which mobilizes fine particles that accumulate on impermeable layers and form a slip plane, particularly across mountainous and hilly terrain with steep to very steep slopes. More details can be seen in **figure 4** below.

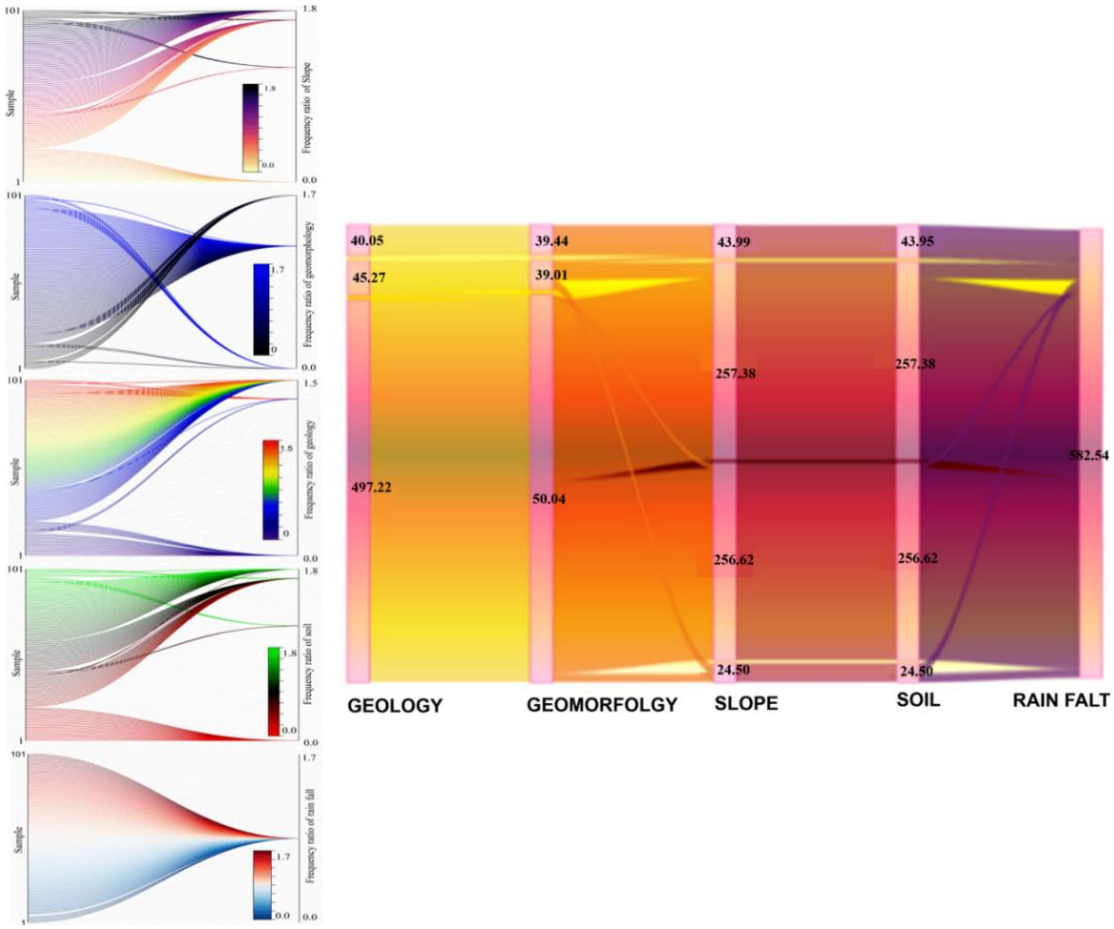

Fig. 3. FR values for each landslide determinant parameter (geology, geomorphology, slope, soil, and rainfall).

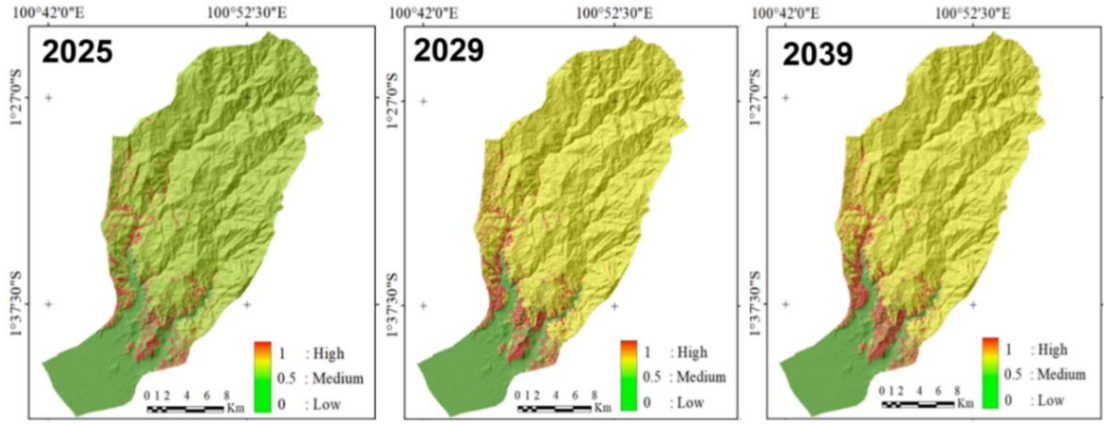

Fig. 4. Landslide hazard model for 2025, 2029, and 2039.

The map in **figure 4** above shows that the LULC conversion coincides with the expansion of landslide-prone areas, especially on steep to very steep slopes. The high-hazard class increases from 4,273.29 ha (8.90%) in 2025 to 4,782.06 ha (9.96%) in 2029 (+508.77 ha; +1.06 percentage points), and to 5,041.89 ha (10.50%) in 2039 (+259.83 ha; +0.54 percentage points). The medium-hazard class rises from 6,134.22 ha (12.78%) in 2025 to 12,820.50 ha (26.70%) in 2029, then moderates to 11,249.37 ha (23.43%) in 2039, remaining well above 2025 levels. Consequently, the low-hazard class shrinks from 37,607.04 ha (78.32%) to 30,411.99 ha (63.34%), before a slight rebound to 31,723.29 ha (66.07%) in 2039. These shifts are concentrated where forests are replaced by oil palm, mixed orchard, and dryland agriculture, which collectively reduce slope reinforcement and surface roughness. More details can be seen in **table 2** below.

Table 2

Changes in landslide hazard areas, 2025–2039.

Landslide class	2025 – Area			2029 – Area			2039 – Area		
	Pixels	Area (ha)	% Area	Pixels	Area (ha)	% Area	Pixels	Area (ha)	% Area
Low	417,856	37,607.04	78.32	337,911	30,411.99	63.34	352,481	31,723.29	66.07
Medium	68,158	6,134.22	12.78	142,45	12,820.50	26.70	124,993	11,249.37	23.43
High	47,481	4,273.29	8.90	53,134	4,782.06	9.96	56,021	5,041.89	10.50
TOTAL	533,495	48,014.55	100.00	533,495	48,014.55	100.00	533,495	48,014.55	100.00

Source: Data analysis, 2025.

Table 2 shows landslide-hazard classes in the Kambang watershed across three years. The modeled extent remains constant at 48,014.55 ha (equivalent to 533,495 pixels) in all years, so the shifts reflect reallocation among classes rather than changes in total area. In 2025, the low class dominates (37,607.04 ha; 78.32%), followed by medium (6,134.22 ha; 12.78%) and high (4,273.29 ha; 8.90%). By 2029, the low class declines sharply to 30,411.99 ha (63.34%), while the medium class increases to 12,820.50 ha (26.70%) and the high class rises to 4,782.06 ha (9.96%). In 2039, the low class recovers slightly to 31,723.29 ha (66.07%), the medium class decreases to 11,249.37 ha (23.43%) yet remains above 2025, and the high class continues to grow to 5,041.89 ha (10.50%). Viewed as period-to-period changes, the high class increases by +508.77 ha (+1.06 percentage points) from 2025 to 2029 and by +259.83 ha (+0.54 percentage points) from 2029 to 2039, yielding a cumulative +768.60 ha (+1.60 percentage points) over 2025–2039. The medium class jumps by +6,686.28 ha (+13.92 percentage points) in 2025–2029, then declines by −1,571.13 ha (−3.27 percentage points) in 2029–2039, remaining +5,115.15 ha (+10.65 percentage points) above its 2025 level. Consequently, the lowclass contracts by −7,195.05 ha (−14.98 percentage points) in 2025–2029 and then rebounds by +1,311.30 ha (+2.73 percentage points) in 2029–2039; overall, it is still 5,883.75 ha smaller than in 2025 (−12.25 percentage points). These trends are consistent with the preceding LULC modeling.

Where conversion of primary/secondary forests to oil palm, mixed orchard, and dryland agriculture tends to occur on steep to very steep slopes, which reduces root reinforcement and surface roughness. In contrast, the low class persists mainly on gently sloping footslopes and valley floors. The results indicate that mitigation priorities should focus on expanding medium–high pockets through deep-rooted revegetation, improved surface and subsurface drainage, and stricter land-use controls in newly converting zones.

4.3 Prediction model for potential landslides

The prediction of LP in the Kambang watershed is controlled by a set of environmental parameters, including Euclidean distance to mapped landslide points as well as the spatial distribution of past landslide points. These layers provide the conditioning context that governs where instability is likely to emerge. More details can be seen in **figure 5** below.

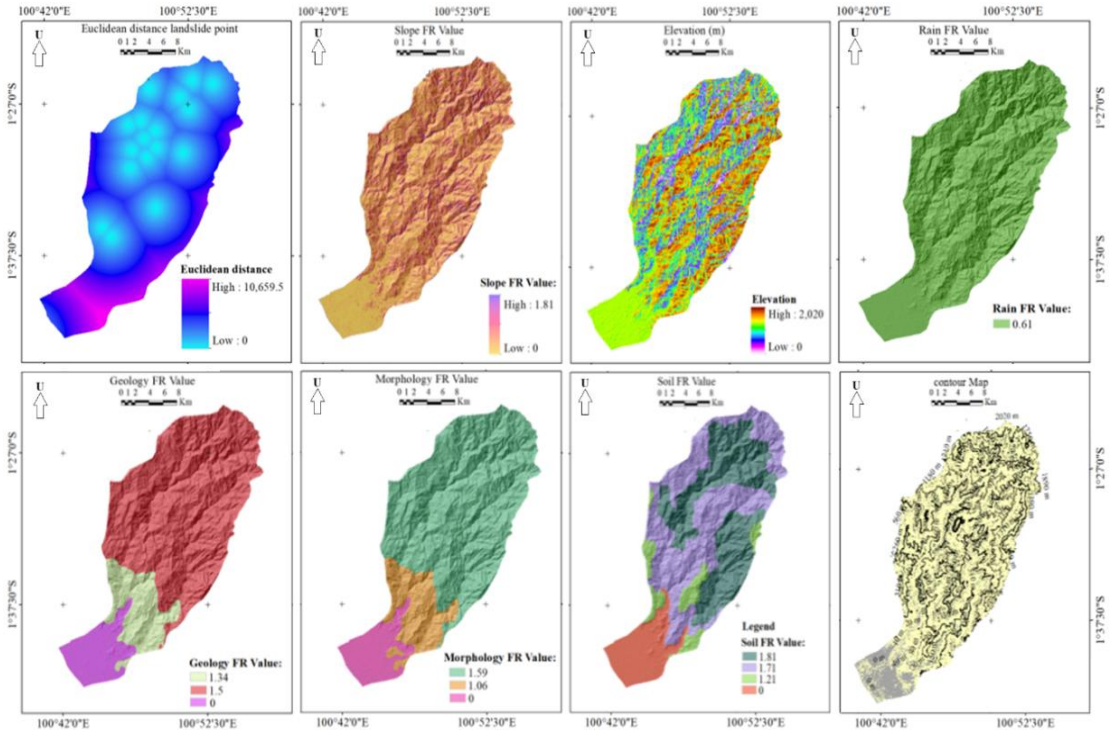

Fig. 5. Environmental parameters for predicting LP.

The maps in **figure 5** above shows, the euclidean distance to landslide points is the most immediate indicator of local susceptibility. The closer a location is to existing landslide points, the higher the potential for new failures. The slope FR shows that steeper gradients are associated with increased likelihood of landsliding. Elevation and contour data reveal strong relief across the basin, ranging from 0 to 2,020 MASL. Higher and more dissected terrain corresponds to steeper slopes and greater runoff concentration. The soil, geology, and geomorphology FR layers indicate that substrate erodibility and landform context affect how water moves through and over the ground. Weathered lithologies and hilly–mountainous landforms permit infiltration, mobilize fine particles, and promote their accumulation on less permeable layers where slip planes can form. The rainfall FR clusters around 0.61, which suggests a relatively uniform spatial distribution of rainfall in the modeling classes. Rainfall therefore acts primarily as a trigger that amplifies instability in areas already conditioned by steep slopes and susceptible materials. To examine interactions among variables and how they intersect with LULC dynamics, we summarize the multi-parameter relationships in a matrix for 2025, 2029, and 2039. More details can be seen in **figure 6**.

The matrix in **figure 7** above shows consistent patterns across time:

1) high slope FR co-occurs with short euclidean distances, indicating spatial clustering of failures along steep valley sides and dissected hillslopes;

2) soil and geology FR classes with greater erodibility tend to align with higher slope FR, pointing to coupled mechanical and hydrological controls on instability;

3) rainfall FR exhibits limited separation among classes.

However, pixels that pair steep slopes with susceptible soils or lithologies display stronger associations. When overlaid with the LULC scenarios, these multi-parameter clusters increasingly intersect areas where forest is replaced by oil palm, mixed orchard, and dryland agriculture, especially on steep to very steep terrain. This convergence explains the subsequent expansion of medium–high hazard pockets and motivates integrating the conditioning parameters with LULC projections in the susceptibility modeling that follows. More details can be seen in **figure 7**.

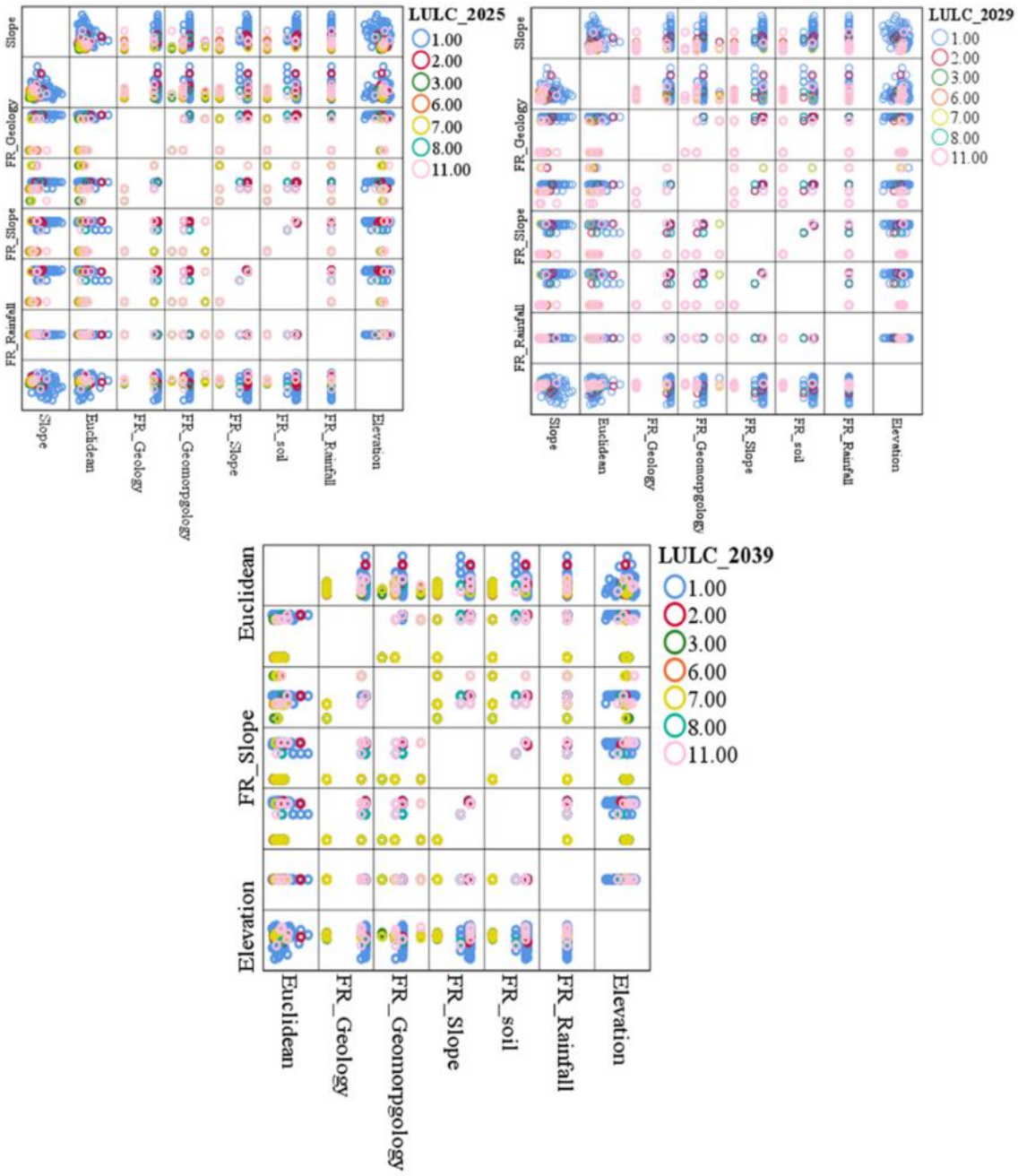

Fig. 6. Environmental-parameter matrix and LULC changes in the Kambang watershed from 2025 to 2039.

The moderate class expands from 6,066.09 ha (12.63%) in 2025 to 10,876.18 ha (22.65%) in 2029 and 11,181.24 ha (23.29%) in 2039. The high class increases from 4,205.16 ha (8.76%) in 2025 to 4,713.93 ha (9.82%) in 2029 and 4,973.76 ha (10.36%) in 2039. Combined, the moderate + high categories grow from 10,271.25 ha (21.39%) in 2025 to 15,590.11 ha (32.47%) in 2029 (+5,318.86 ha; +11.08 percentage points), and to 16,155.00 ha (33.65%) in 2039 (+564.89 ha; +1.18 percentage points). To evaluate whether the modeling results are acceptable, we computed the ROC/AUC metrics for each year. The AUC values are 0.95 (2025), 0.87 (2029), and 0.84 (2039).

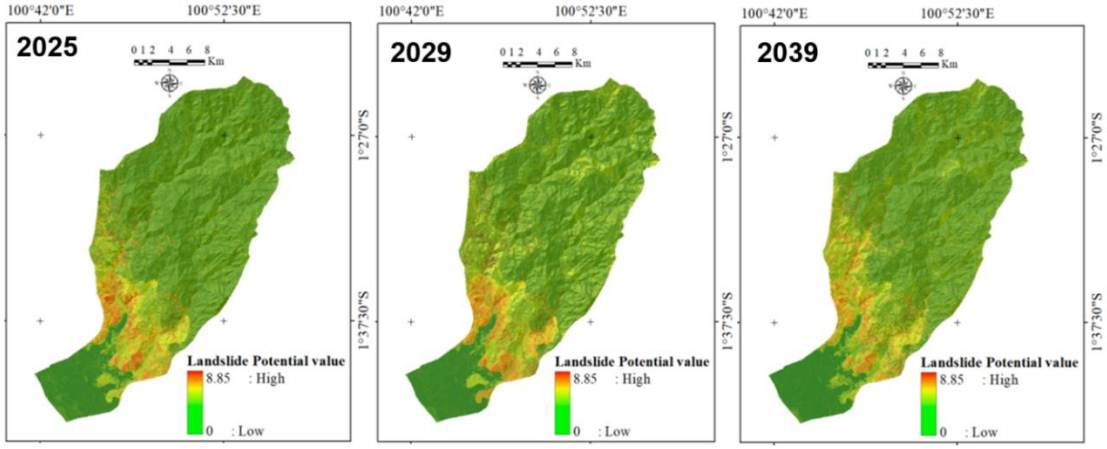

Fig. 7. Predicted LP maps for 2025, 2029, and 2039 in the Kambang watershed.

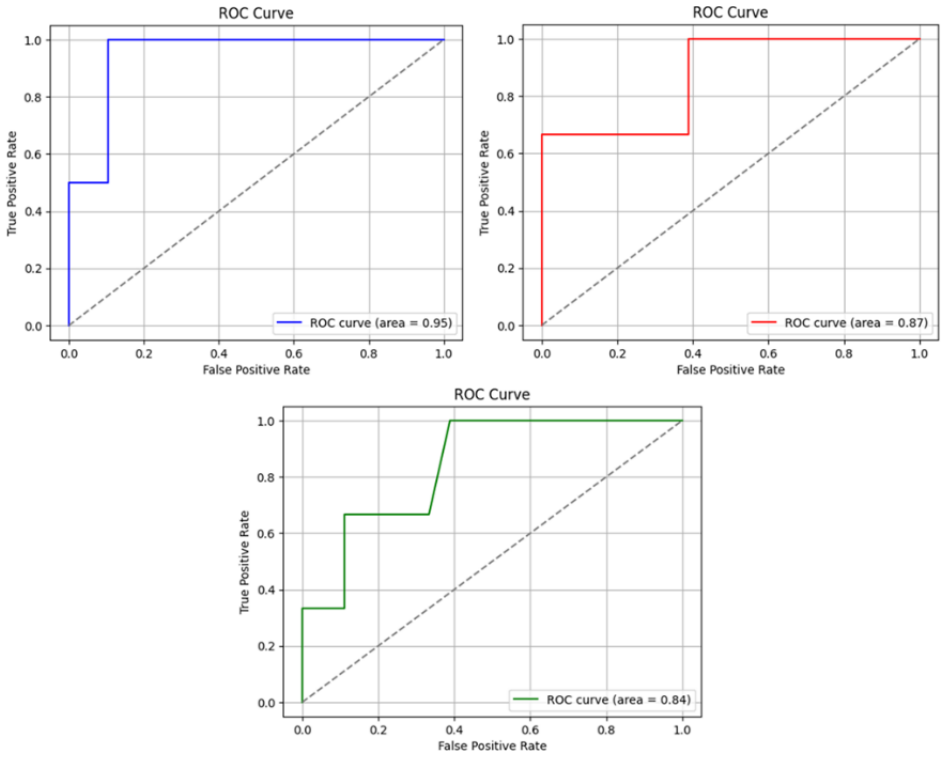

Fig. 8. ROC curves (AUC) for the landslide-potential models in 2025, 2029, and 2039.

The graph in **figure 8** above shows ROC curves that evaluate how well the models distinguish landslide from non-landslide pixels. The diagonal gray line marks random performance (AUC = 0.50); curves farther above this line indicate better discrimination. The 2025 model (blue) achieves AUC = 0.95, reflecting excellent accuracy with high true-positive rates at low false-positive rates. The 2029 model (red) attains AUC = 0.87, indicating good performance, while the 2039 model (green) yields AUC = 0.84, indicating moderate–good discrimination and greater uncertainty at the longer projection horizon. Overall, the models are suitable for planning and prioritization, with added caution recommended for the later years and periodic updates as new data becomes available.

DISCUSSION

The LULC change in the Kambang watershed is largely human-driven to meet household needs and livelihood strategies (Patel et al., 2024; Van Toor et al., 2024; Zhu et al., 2025). In practice, communities intensify agriculture even on steep to very steep slopes by converting primary and secondary forest into agricultural fields, mixed orchards, and oil-palm plantations, thereby altering natural cover and slope hydrology (Kubacka et al., 2025; Kasahun, 2025; Kafy et al., 2021). During rainy periods, land clearing facilitates downward migration of fine particles; these accumulate on relatively impermeable layers and form slip planes, especially where clayey textures are present, which increases landslide likelihood (Asada et al., 2024; Asmare, 2023).

Our hazard analysis confirms that landslide susceptibility reflects multiple conditioning factors, namely geology, geomorphology, slope, soil, rainfall, and LULC and their joint uncertainty (Huang et al., 2024; Wei et al., 2024). Changes in LULC, therefore, translate into changes in the hazard footprint (Girma et al., 2022; Kafy et al., 2021; Ghalehteimouri et al., 2022). Recent morphodeformation analysis using Sentinel-1A SAR along the Singkarak segment demonstrates how remote-sensing deformation signals can be integrated with geospatial hazard layers to sharpen the delineation of instability zones, supporting the coupling of dynamic LULC with susceptibility mapping in data-limited settings (Triyatno et al., 2025). In Kambang, the high-hazard class increases by 508.77 ha (+1.06 percentage points) from 2025→2029 and 259.83 ha (+0.54 pp) from 2029→2039. When moderate and high are combined, the at-risk area expands by 5,318.86 ha (+11.08 pp) in 2025→2029 and a further 564.89 ha (+1.18 pp) in 2029→2039.

Although much of the watershed remains in the low class, these increments are spatially concentrated on dissected hillslopes where forest conversion is occurring. Policy responses should therefore prioritize regulating land conversion on steep forested slopes, deep-rooted revegetation, and surface–subsurface drainage improvements, coupled with community education around forest-edge areas (Mondal et al., 2016; Lausch et al., 2025; Kasahun, 2025). Experience from the Tarusan watershed shows that GIS-based prioritization and community-oriented mitigation (e.g., structural drainage, vegetative buffers, and zoning enforcement) are effective for reducing compound hydro-geomorphic risks, offering an operational template for Kambang's steep-slope management (Umar & Triyatno, 2024). The prediction model for LP integrates environmental parameters with mapped landslide points and shows that projected LULC trajectories will continue to reshape susceptibility hot spots (Williams et al., 2025; Zandi & Shah Pari Far, 2025; Naeem et al., 2025). Increases are most pronounced where forest gives way to oil palm, mixed orchard, and dryland agriculture on steep terrain, processes that elevate erosion risk and soil saturation, proximate precursors to slope failure (Talukdar et al., 2021; Zhou et al., 2021).

CONCLUSIONS

The results indicate a clear and coherent trajectory linking LULC change to evolving landslide susceptibility in the Kambang watershed. Between 2025 and 2039, primary forest declines from 36,742.23 ha (76.52%) to 33,310.80 ha (69.38%), while secondary forest contracts from 4,070.07 ha (8.48%) to 2,858.04 ha (5.95%). In contrast, oil palm expands sharply to 3,920.49 ha (8.17%) by 2039, accompanied by gradual growth in mixed orchard and dryland agriculture. Built-up land, rice fields, mangrove, and water bodies remain essentially stable. Spatially, oil palm concentrates on gentler terrain and valley floors, whereas conversions affecting forest classes advance onto dissected hillslopes often below ~500 MASL, where removal of deep-rooted vegetation diminishes slope reinforcement during peak rainy seasons. These LULC trajectories translate into a measurable redistribution of landslide hazard.

The low-hazard class shrinks overall by 5,883.75 ha (−12.25 percentage points) from 2025 to 2039, while the medium class remains ~5,115.15 ha (+10.65 pp) above its 2025 level and the high class grows cumulatively by 768.60 ha (+1.60 pp). Combined, the moderate + high footprint expands from 21.39% in 2025 to 33.65% in 2039. Frequency-ratio diagnostics clarify the controls: slope and soil contain the strongest positive associations (to ~1.81), geomorphology and geology contribute

secondary effects, and rainfall clustered near an FR of ~0.61 acts chiefly as a trigger that amplifies instability where conditioning factors are already adverse. The most hazardous configurations occur where steep slopes intersect susceptible substrates and recent forest loss. Model skill supports these interpretations. The LULC classifications achieve overall accuracies of 0.92 (2025), 0.88 (2029), and 0.86 (2039), exceeding accepted thresholds for downstream applications. Landslide-potential predictions yield AUC values of 0.95, 0.87, and 0.84 for 2025, 2029, and 2039, respectively, ranging from excellent to moderate-good discrimination, with uncertainty increasing at longer years. Taken together, the evidence shows that continued forest conversion on steep terrain is the primary driver of expanding susceptibility.

To mitigate future risks, priority actions should include protecting steep-slope forests, deploying deep-rooted revegetation and targeted slope stabilization, upgrading surface–subsurface drainage on hillslopes and along access roads, and incorporating the 2025/2029/2039 susceptibility maps into risk-sensitive spatial planning. Routine monitoring, community education at forest–agriculture interfaces, and periodic model updates as new observations accrue will be essential to keep risk reduction aligned with the basin's rapidly changing land systems.

ACKNOWLEDGEMENTS

The author gratefully acknowledges the academic community of Universitas Negeri Padang for their invaluable assistance with data collection, data processing, and the preparation of spatial datasets. The author also extends thanks to the Institute for Research and Community Service (LP2M), Universitas Negeri Padang, for funding this research through the "Research Collaboration with Foreign Universities" scheme under Contract No. 1845/UN35.15/LT/2025.

REFERENCES

Ahmad, M. S., Monalisa, & Khan, S. (2023). Comparative analysis of analytical hierarchy process (AHP) and frequency ratio (FR) models for landslide susceptibility mapping in Reshun, NW Pakistan. Kuwait Journal of Science, 50(3), 387–398. DOI: 10.1016/j.kjs.2023.01.004

Asada, H., Hasegawa, Y., & Minagawa, T. (2024). Development of shallow landslide susceptibility maps incorporating relative spacing index for forest management. Environmental and Sustainability Indicators, 24, 100515. DOI: 10.1016/j.indic.2024.100515

Asmare, D. (2023). Application and validation of AHP and FR methods for landslide susceptibility mapping around Choke Mountain, northwestern Ethiopia. Scientific African, 19, e01470. DOI: 10.1016/j.sciaf.2022.e01470

Badrakh, M., Tserendash, N., Choindonjamts, E., & Albert, G. (2025). Potential of random forest machine learning algorithm for geological mapping using PALSAR and Sentinel-2A remote sensing data: A case study of Tsagaan-uul area, southern Mongolia. Journal of Asian Earth Sciences: X, 14, 100204. DOI: 10.1016/j.jaesx.2025.100204

Barlian, E., Umar, I., Dewata, I., Triyatno., Putra, A., Mustikasari, E., Purnamaningtyas, S. E., Hendrajat, E. A., Sari, S. M., Yulius, Y., & Siregar, D. R. (2025). GIS and AHP-based flood zoning and conservation strategies in the Tarusan watershed, Indonesia. Geographia Technica, 20(2), 114–133. DOI: 10.21163/GT_2025.202.08

Beroho, M., Yousfi, M., Chehbouni, M., El Housni, H., Khaoulani, M., Mjahed, H., El Moatamid, A., Hakmi, M., Ait El Abdoun, A., &Soulaimani, A. E. M. (2025). A novel SWAT-based framework to integrate climate and LULC scenarios for predicting hydrology and sediment dynamics in the watersheds of Mediterranean ecosystems. Journal of Environmental Management, 388, 125446. DOI: 10.1016/j.jenvman.2025.125446

Chowdhury, Md. S., Rahman, Md. N., Sheikh, Md. S., Sayeid, Md. A., Mahmud, K. H., & Hafsa, B. (2024). GIS-based landslide susceptibility mapping using logistic regression, random forest and decision and regression tree models in Chattogram District, Bangladesh. Heliyon, 10(1), e23424. DOI: 10.1016/j.heliyon.2023.e23424

Es-smairi, A., Elmoutchou, B., Mir, R. A., OuazaniTouhami, A. E., &Namous, M. (2023). Delineation of landslide susceptible zones using frequency ratio (FR) and Shannon entropy (SE) models in northern Rif, Morocco. Geosystems and Geoenvironment, 2(4), 100195. DOI: 10.1016/j.geogeo.2023.100195

Febriandi., Fatimah, S., Triyatno,., Hermon, D., Putra, A., Mutmainah, H., Arifin, T., &Akhwady, R. (2025). Predicting of land cover changes until 2030 and assessing sustainability status in the Mandeh region, Indonesia. *GeographiaTechnica, 20*(1), 263–280. DOI: 10.21163/GT_2025.201.18

Ghalehteimouri, K. J., Shamsoddini, A., Mousavi, M. N., Che Ros, F. B., &Khedmatzadeh, A. (2022). Predicting spatial and decadal of land use and land cover change using integrated cellular automata Markov chain model based scenarios (2019–2049) Zarriné-Rūd River Basin in Iran. Environmental Challenges, 6, 100399. DOI: 10.1016/j.envc.2021.100399

Girma, R., Fürst, C., &Moges, A. (2022). Land use land cover change modeling by integrating artificial neural network with cellular automata-Markov chain model in Gidabo river basin, main Ethiopian rift. Environmental Challenges, 6, 100419. DOI: 10.1016/j.envc.2021.100419

Huang, F., Wang, Y., Chen, J., Wu, C., Fang, Z., & Hong, H. (2024). Uncertainties of landslide susceptibility prediction: Influences of random errors in landslide conditioning factors and errors reduction by low pass filter method. Journal of Rock Mechanics and Geotechnical Engineering, 16(1), 213–230. DOI: 10.1016/j.jrmge.2023.11.001

Ikhwan., Triyatno., Putra, A., & Syah, N. (2025). Dynamics of LULC changes in communal lands: A socio-cultural and spatial analysis in Bukittinggi City, Indonesia. Geographia Technica, 20(1), 112–126. DOI: 10.21163/GT_2025.201.09

Kafy, A.-A., Dey, N. N., Al Rakib, A., Rahaman, Z. A., Nasher, N. M. R., & Bhatt, A. (2021). Modeling the relationship between land use/land cover and land surface temperature in Dhaka, Bangladesh using CA-ANN algorithm. Environmental Challenges, 4, 100190. DOI: 10.1016/j.envc.2021.100190

Kasahun, M. (2025). Quantifying deforestation drivers through multi-temporal LULC analysis and population-forest correlation modeling: A case study of Dara Woreda, Ethiopia. Environmental Challenges, 19, 101163. DOI: 10.1016/j.envc.2025.101163

Kubacka, M., Piniarski, W., Żywica, P., & Frazier, A. E. (2025). Tracking spatio-temporal LULC changes in key ecological network elements using fragmentation metrics and a custom raster-based approach: A multi-scale study from Poland. Ecological Informatics, 90, 103369. DOI: 10.1016/j.ecoinf.2025.103369

Lausch, A., Selsam, P., Heege, T., von Trentini, F., Almeroth, A., Borg, E., Klenke, R., &Bumberger, J. (2025). Monitoring and modelling landscape structure, land use intensity and landscape change as drivers of water quality using remote sensing. Science of The Total Environment, 960, 178347. DOI: 10.1016/j.scitotenv.2024.178347

Mondal, Md. S., Sharma, N., Garg, P. K., &Kappas, M. (2016). Statistical independence test and validation of CA Markov land use land cover (LULC) prediction results. The Egyptian Journal of Remote Sensing and Space Science, 19(2), 259–272. DOI: 10.1016/j.ejrs.2016.08.001

Murmu, J., Radhadevi, L., Pande, C., Bandaru, M., & Kumar, M. (2025). Indicators of sustained agriculture, impacts of LULC and weather parameters on ET: Case study in Chota Nagpur Plateau. Environmental and Sustainability Indicators, 27, 100836. DOI: 10.1016/j.indic.2025.100836

Naeem, M., Liu, C., Shafi, M., Iqbal, J., Shikhawat, A. F., Rao, Z., Ahbia, A., Anşari, M., Baloch, W. U., & Niaz, A. (2025). Assessing and predicting Bojiang lake area and LULC changes from 2000 to 2045. Journal of Hydrology: Regional Studies, 58, 102216. DOI: 10.1016/j.ejrh.2025.102216

Patel, A., Vyas, D., Chaudhari, N., Patel, R., Patel, K., & Mehta, D. (2024). Novel approach for the LULC change detection using GIS & Google Earth Engine through spatiotemporal analysis to evaluate the urbanization growth of Ahmedabad city. Results in Engineering, 21, 101788. DOI: 10.1016/j.rineng.2024.101788

Putra, A., Hermon, D., Dewata, I., Barlian, E., & Triyanto. (2025). USLE method for erosion prediction and conservation measures at the Air Dingin watershed of the upstream part in Padang City, Indonesia. In Erosion Measurement, Modeling, and Management: Challenges and Solutions. 123–148. Apple Academic Press. DOI: 10.1201/9781003494508_6

Rodríguez-Ortega, J., Tabik, S., Benhammou, Y., Khaldi, R., & Alcaraz-Segura, D. (2025). Land use and land cover fraction estimation for Sentinel-2 RGB images: A new LULC mapping task. Remote Sensing Applications: Society and Environment, 39, 101626. DOI: 10.1016/j.rsase.2025.101626

Roy, D., Sarkar, A., Kundu, P., Paul, S., & Chandra Sarkar, B. (2023). An ensemble of evidence belief function (EBF) with frequency ratio (FR) using geospatial data for landslide prediction in Darjeeling Himalayan region of India. Quaternary Science Advances, 11, 100092. DOI: 10.1016/j.qsa.2023.100092

Shanley, C. S., Eacker, D. R., Reynolds, C. P., Bennetsen, B. M. B., & Gilbert, S. L. (2021). Using LiDAR and random forest to improve deer habitat models in a managed forest landscape. Forest Ecology and Management, 499, 119580. DOI: 10.1016/j.foreco.2021.119580

Talukdar, S., Eibek, K. U., Akhter, S., Ziaul, S., Md. Towfiqul Islam, A. R., & Mallick, J. (2021). Modeling fragmentation probability of land-use and land-cover using the bagging, random forest and random subspace in the Teesta River Basin, Bangladesh. Ecological Indicators, 126, 107612. DOI: 10.1016/j.ecolind.2021.107612

Triyatno., Bert, I., Idris., Hermon, D., & Putra, A. (2020). Hazards and morphometry to predict the population loss due to landslide disasters in Koto XI Tarusan – Pesisir Selatan. International Journal of GEOMATE, 19(76), 98–103. DOI: 10.21660/2020.76.ICGeo12

Triyatno., Berd, I., & Idris. (2023). Spatial model of flood hazard due to land cover change in the Tarusan watershed, West Sumatra—Indonesia. International Journal of GEOMATE, 25(108), 21–29. DOI: 10.21660/2023.108.3774

Triyatno., Anwar, S., Febriandi., & Rahmi, L. (2024). GIS based on analysis of earthquake hazard level using the PGA in Siberut–Mentawai Islands Regency for sustainability in disaster mitigation. Journal of Sustainability Science and Management, 19(12), 107–119. DOI: 10.46754/jssm.2024.12.007

Triyatno., Caesario, D., Febriandi., Aulia, B., & Syarief, A. (2025). Predicting earthquake potential through morphodeformation modeling using Sentinel-1A imagery in the Singkarak segment, Indonesia. Geographia Technica, 20(2), 190–204. DOI: 10.21163/GT_2025.202.12

Umar, I., & Triyatno. (2024). Flood hazard mitigation at Tarusan Watershed, South Pesisir District, West Sumatera Province. Jurnal Pengelolaan Sumberdaya Alam dan Lingkungan, 14(1), 101–108. DOI: 10.29244/jpsl.14.1.101-108

Van Toor, M. L., Davranche, A., Delaunay, G., Murgue, C., Waldenström, J., &Arzel, C. (2024). An evaluation of global LULC maps for the estimation of habitat use of a declining migratory waterbird along its flyway. SSRN. DOI: 10.2139/ssrn.5037387

Wei, Y., Qiu, H., Liu, Z., Huangfu, W., Zhu, Y., Liu, Y., Yang, D., & Kamp, U. (2024). Refined and dynamic susceptibility assessment of landslides using InSAR and machine learning models. Geoscience Frontiers, 15(6), 101890. DOI: 10.1016/j.gsf.2024.101890

Williams, C., Whitbread, K., Hall, A., Roberson, S., Finlayson, A., Palamakumbura, R. N., Hulbert, A., &Paice, M. (2025). Capturing exposed bedrock in the upland regions of Great Britain: A geomorphometric focused random forest approach. Computers & Geosciences, 196, 105814. DOI: 10.1016/j.cageo.2024.105814

Zandi, R., & Shah Pari Far, G. (2025). Evaluating the factors affecting landslides using machine learning algorithms (case study: The catchment area of Karun-3 Dam, Iran). The Egyptian Journal of Remote Sensing and Space Sciences, 28(3), 512–522. DOI: 10.1016/j.ejrs.2025.07.005

Zhou, X., Wen, H., Zhang, Y., Xu, J., & Zhang, W. (2021). Landslide susceptibility mapping using hybrid random forest with GeoDetector and RFE for factor optimization. Geoscience Frontiers, 12(5), 101211. DOI: 10.1016/j.gsf.2021.101211

Zhu, Y., [add remaining authors]. (2025). Analysis and prediction of spatiotemporal carbon storage changes in the Taihu Lake Basin in Jiangsu Province based on PLUS and InVEST model. Trees, Forests and People, 100916. DOI: 10.1016/j.tfp.2025.100916